Draft version November 9, 2018
Preprint typeset using LaTeX style AASTeX6 v. 1.0

THE SHORT TERM STABILITY OF A SIMULATED DIFFERENTIAL ASTROMETRIC REFERENCE FRAME IN THE GAIA ERA

Ummi Abbas[1], Beatrice Bucciarelli, Mario G. Lattanzi, Mariateresa Crosta, Mario Gai, Richard Smart, Alessandro Sozzetti, Alberto Vecchiato

Osservatorio Astrofisico di Torino
Via Osservatorio 20
Pino Torinese, I-10025, Italy

[1]abbas@oato.inaf.it

ABSTRACT

We use methods of differential astrometry to construct a small field inertial reference frame stable at the micro-arcsecond level. Such a high level of astrometric precision can be expected with the end-of-mission standard errors to be achieved with the Gaia space satellite using global astrometry. We harness Gaia measurements of field angles and look at the influence of the number of reference stars and the star's magnitude as well as astrometric systematics on the total error budget with the help of Gaia-like simulations around the Ecliptic Pole in a differential astrometric scenario.
We find that the systematic errors are modeled and reliably estimated to the μas level even in fields with a modest number of 37 stars with G <13 mag over a 0.24 sq.degs. field of view for short time scales of the order of a day with high-cadence observations such as those around the North Ecliptic Pole during the EPSL scanning mode of Gaia for a perfect instrument. The inclusion of the geometric instrument model over such short time scales accounting for large-scale calibrations requires fainter stars down to G = 14 mag without diminishing the accuracy of the reference frame. We discuss several future perspectives of utilizing this methodology over different and longer timescales. [a]

Keywords: astrometry – methods: data analysis – methods: statistical – reference systems

1. INTRODUCTION

The principles of differential astrometry can be used in a variety of applications: e.g. for improving the origin of a fundamental star-catalog coordinate system (Zverev 1976) with the help of differential astrometric observations of the Sun and planets; cluster membership studies that can be performed using relative proper motions and even in deriving absolute proper motions of globular clusters and distant open clusters (van Altena et al. 2013; Dinescu et al. 1997); detecting the reflex motion of the target star due to the presence of its planets (Sozzetti 2005); obtaining trigonometric parallaxes (Benedict et al. 2002, 2009; McArthur et al. 2011, 1999; Riess et al. 2014; Casertano et al. 2016) or measuring the relativistic deflection due to the various moments of massive planets and in determining PPN-γ (Crosta & Mignard 2006).

The preliminary step before studying such 'differential' effects involves the establishment of a reliable 'local' inertial reference frame which we attempt in this paper. In general, a 'global' reference frame is defined by the positions of objects through their coordinates in a reference system (a coordinate system specifying the direction of the axes and the zero point or the origin) and thereby represents a practical realization of the reference system (Johnston & de Vegt 1999). For example, the International Celestial Reference Frame (ICRF) is the realization of the International Celestial Reference System (ICRS) and thereby defines the directions of its axes. At different wavelengths the precision of the ICRS-axes orientation varies reaching ∼10 micro-arcsecond (μas) at radio frequencies, leading to the second realization of the ICRF, i.e. ICRF2, and milli-arcseconds (mas) at optical wavelengths. At radio frequencies, the ICRF is defined mainly by very distant extragalactic sources having no discernible proper motions leading to the definition of a quasi-inertial reference frame. On the other hand, for small fields (∼ 1 square degree on the sky) the local reference frame is inertial in the sense that the po-

[a] This is an author-created, un-copyedited version of an article accepted for publication in Publications of the Astronomical Society of the Pacific. The publisher is not responsible for any errors or omissions in this version of the manuscript or any version derived from it. The Version of Record is available online at [DOI TBC].

sitions and motions of an object that are due to forces acting on the objects can be reliably modeled within the random measurement errors (Treuhaft & Lowe 1990).

It is desirable to use many fixed and stable points to define a reliable local reference frame even though in principle a couple of points are enough, e.g. right ascension and declination describing the angular distance from the origin of right ascension and from the catalog equator respectively (Johnston & de Vegt 1999). A modern astrometric catalog contains data on a large number of objects, so the coordinate system is vastly overdetermined but allows to decrease the 'random' measurement error by a factor of the square root of the total number of observations. The rms scatter of repeated observations of the positions of these objects in a given reference frame define its stability. Typically, every catalog contains systematic errors, i.e. errors in position that are similar in direction and magnitude for objects sharing similar characteristics, lying in the same area of the sky, or are of the same magnitude (flux) or color (spectral index). Systematic errors lead to biases in the reference frame that is effectively different for different classes of objects. Obviously, minimizing systematic errors through good physical models when a catalog is constructed is as important, if not more so, than minimizing the random errors.

In the presence of Earth's atmosphere, limitations to the astrometric precision are caused by effects such as refraction, turbulence, delays, etc (Sozzetti 2005). In its absence, for space-based measurements and for those that are differential in nature (based on reference objects that are all within a small field), we need to address effects such as: light aberration that is of the order of $\sim$20 arcseconds to first order and a few mas to second order (Klioner 2003); gravitational deflection terms that lead to effects of several mas even at the Ecliptic Pole due to the monopole moment of the Sun (Crosta & Mignard 2006; Turyshev 2002); parallaxes and proper motions of stars that can be either removed apriori or accounted for in the model (van Altena et al. 2013); and for changes in the geometric instrument model due to thermal variations and imperfections in the instrument that need to be efficiently calibrated (Lindegren et al. 2012).

In this paper we use Gaia-like simulations that are optimized for global astrometry and study the measurements with a differential astrometric approach. We analyze the efficiency of such a method in constructing a high-precision inertial astrometric reference frame over small fields whose size is determined by the dimensions of Gaia's field of view. We describe the total error budget in terms of various systematics due to different astrometrical effects, astrophysical effects due to the star's magnitude, and geometrical effects due to the distribution of a given number of stars.

The paper is divided into the following sections: In Sec. 2 we describe the details of the simulation set-up, Sec. 3 presents the properties of a space-based differential reference frame, the following Sec. 4 discusses the principles of Differential Astrometry alongwith the applied astrometric modeling in Sec. 5 and some of the results obtained (Sec. 5.1.1) and their Discussion (Sec. 6) finally wrapping up with Future Perspectives (Sec. 7).

2. THE SIMULATION SET-UP

The Gaia space satellite will perform unprecedented high precision global astrometry at the μarcsecond level of roughly 1 billion stars down to G $\sim$ 20 mag. Under such conditions we want to study the potential of differential astrometric measurements in establishing a local reference frame. We use simulated Gaia observations as a testbed for our analysis, which however is general enough to be applied to any scenario with overlapping measurements that can be treated in a differential manner ultimately leading to a reliable local Reference Frame. We attempt this by using the field angles, η and ζ, as measured in the field of view (FOV) of Gaia respectively in the scanning direction of the satellite and perpendicular to it instead of using global coordinates, i.e. positions (α, δ), that will only be obtained after a sphere solution within the framework of absolute astrometry, e.g. the astrometric data from Gaia in its first data release (GDR1, Lindegren et al. 2016).

The simulation is produced with AGISLab, a software package ideal for small-scale experimental runs on a laptop that are realistic and faithful to the Gaia satellite and that uses a subset of the most important functionalities of the AGIS (Astrometric Global Iterative Solution) mainstream pipeline that is used to analyze the real Gaia data (Holl et al. 2012). In fact, much of the code was tested with AGISLab before being implemented in AGIS and results are equivalent to what can be expected with AGIS. For this paper the setup is based on the actual Gaia satellite that is equipped with two field of views (FOVs) separated by a large 'basic angle' (=106.5) rotating at a fixed spin rate of $59.9605" s^{-1}$ around its spin axis (see Gaia Collaboration et al. 2016 for extensive details). In addition, the simulator is run using nominal CCD size, focal plane geometry and FOV size and orbital parameters. The observed source (proper) direction is computed using a suitable relativistic model required for high astrometric accuracies and that includes the parametrized post-Newtonian (PPN) formulation adopted for Gaia (Klioner 2003) taking into account the gravitational light deflection due to solar system bodies and the stellar aberration due to the Lorentz transformation of Gaia's co-moving reference frame further described in Sec. 3.1.1.

The principle of scanning space astrometry allows im-

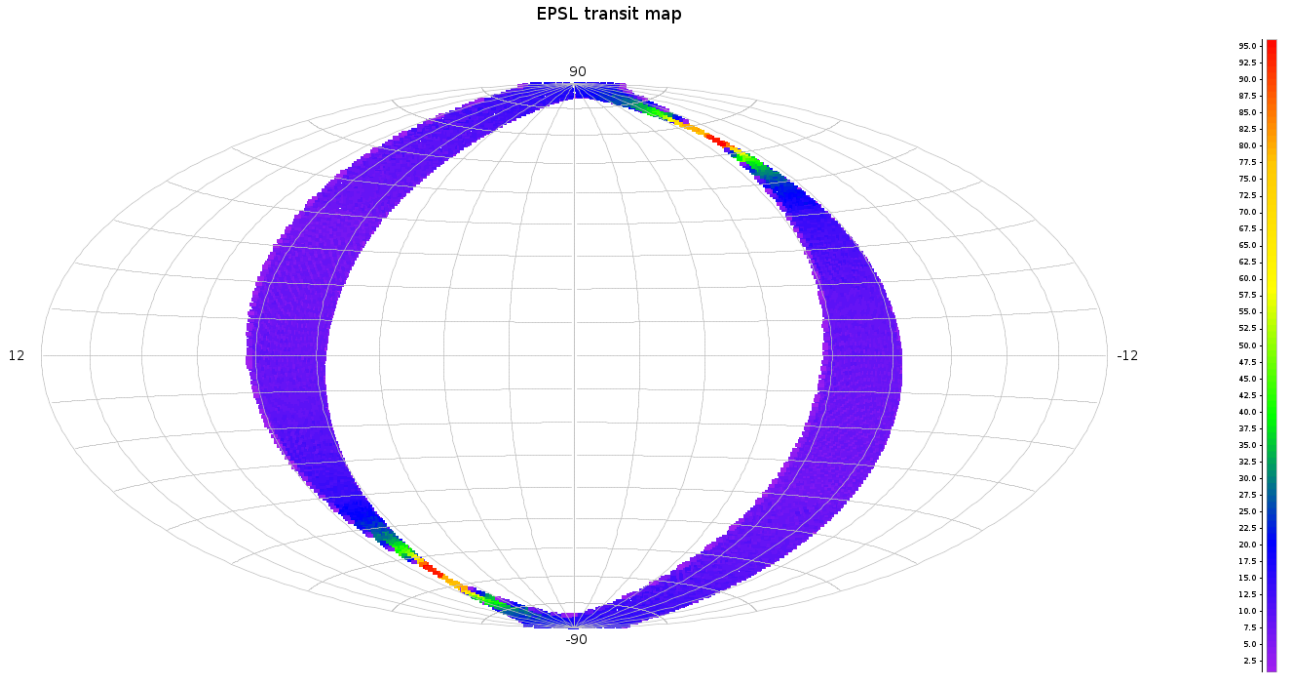

Figure 1. The simulated transit map in equatorial coordinates showing the undisturbed ecliptic pole scanning law executed for 28 days. The different colors correspond to the number of transits quantitatively shown in the color bar.

ages to be mapped onto a common focal plane thereby providing a measure of the time when the object transits (Lindegren & Bastian 2011). These simulated transit times provide the 1-dimensional Along Scan (AL) stellar positions relative to the instrument axes. The scanning law at a fixed solar-aspect angle is determined by two heliotropic angles, the precession phase, $\nu(t)$, given by the angle between the ecliptic plane and the Sun-satellite spin axis plane, and the spin phase, $\omega(t)$, given by the angle between the satellite's z-x plane and the Sun-satellite spin axis plane. The equations governing these angles has two free parameters; the initial spin phase and the initial precession phase at the start of the satellite science operations.

The AGISLab simulation has been setup to account for the nominal mission phase of Gaia that started on 25/7/2014 with the onset of an undisturbed 28 days Ecliptic Pole Scanning Law (EPSL) that allowed for the early calibration of several post-commissioning effects (Gaia Collaboration et al. 2016). The EPSL meant that the ecliptic poles were observed on each full rotation of the satellite, i.e. every 6 hours (Clementini et al. 2016) due to the precession phase being kept constant at 180° (see Fig. 1). After the EPSL the subsequent nominal scanning law was optimized in the initial spin phase and the initial precession phase to favour events of bright stars close to the limb of Jupiter for the relativity light deflection experiment due to Jupiter's quadrupole moment (de Bruijne et al. 2010).

Taking advantage of the short time duration (which we will assume to be $\sim$ 24 hours) and high-cadence observations during EPSL we can further assume that the small-scale along scan (AL) calibrations and large-scale across scan (AC) calibrations either remain stable or are constant over long time scales, in the case of the former even for the whole mission duration (further described in Section 3.2). Successive frames should then present a roto-translation between them that can be studied with the GAUSSFit software (Jefferys et al. 1988), this is further described in the next Section. The input stars are taken from the Initial Gaia Source List (IGSL) star catalogue (Smart & Nicastro 2014) around the North Ecliptic Pole (NEP), this particular field is shown in Fig. 2. In order to use and fit any number of parameters we will use the simulated field angles in the Gaia FOV with the NEP always in the middle, i.e. fifth CCD column in Gaia's FOV. This is illustrated in Fig. 3 where stars with G-magnitudes brighter than 16 in a field of size 0.6x0.4 degrees were selected and are shown superposed on the Astrometric Field of the Gaia Focal Plane. In more detail, the Focal Plane consists of a total of 106 CCDs that make up the Astrometric Field (AF), Blue and Red Photometer and the Radial Velocity Spectrometer. We will be concerned only with the Astrometric measurements provided by the 14 CCDs in the Sky Mappers (SM) and 62 CCDs in the Astrometric Field (AF1-AF9 for a total of 9 CCD columns each with 7 rows of CCDs except for the last column AF9 that has 6 CCD rows). These CCDs have 4500 and 1966 pixel columns in the AL and AC directions respectively.

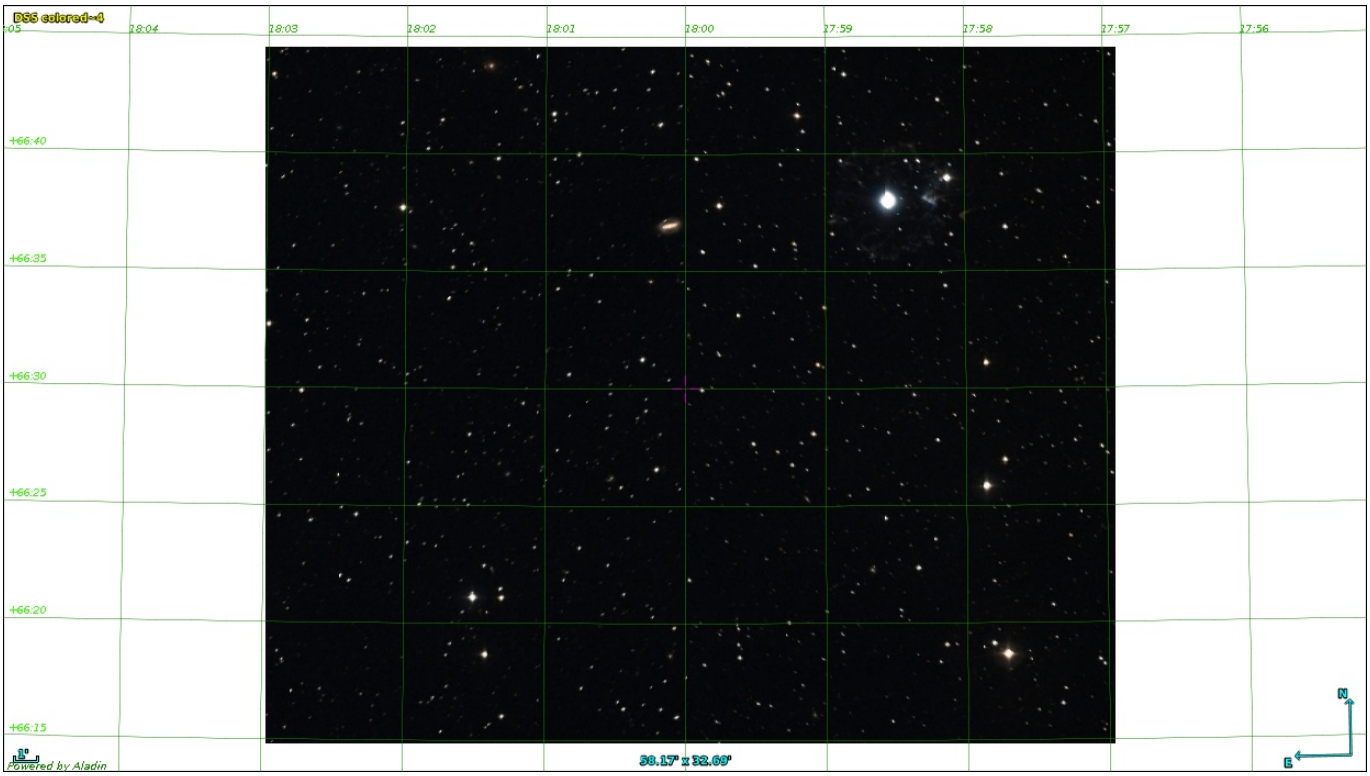

Figure 2. The DSS image of the star field (size $\sim$ 0.5x0.5 degs) around the North Ecliptic Pole courtesy Aladin.

In reality, Gaia will observe in Time-Delayed Integration (TDI) mode with the average speed of the motion of optical images (scan rate of Gaia) equal to the speed of charge flowing along the CCD column. The fundamental observational quantity is given by the time (*tobs*) when a stellar image centroid passes the *fiducial line* of a CCD, which is generally halfway between the first and the last TDI line used in the integration (Lindegren et al. 2012). As we are interested in the configuration of stars at a fixed time, the *tobs* are converted into Along Scan (AL) positions by multiplying with the scan rate after subtraction from a reference time, i.e. the time of observation of the target or reference point (NEP in our case) in the same frame.

Gaia's astrometric instrument is optimized for one-dimensional measurements in the AL, whereas the requirements are much less stringent in the AC direction typically showing up as larger uncertainties in AC observations versus those seen in the AL direction. The standard uncertainty per AL/AC observation is given in Table 1 as a function of the star's magnitude with fainter stars typically having high uncertainties of 383 μ-as in the AL-direction for G = 16 mag stars. Generally, the AC uncertainties are 5-13 times worse for the magnitude range we will be looking at (G $\lesssim$ 16 mag). For what follows it must be kept in mind that stars brighter than G $\lesssim$ 13 mag are always observed as two-dimensional images that give accurate AL and AC positional information, whereas fainter star observations acquired in the Astrometric Field are generally one-dimensional due to the AC position information being removed on-board by on-chip binning. Two dimensional observations at the faint end is only sporadically available for special 'Calibration' Faint Stars and instead are always provided for by the Sky Mappers (SM), albeit with higher uncertainties that nonetheless provide approximate two-dimensional positions of the images.

In order to ensure that the NEP always remains at the center of the FOV surrounded by the same set of stars that define the local Reference Frame, the observing times of the set of stars is restricted to within $\pm$15 seconds of the NEP *tobs* for the same CCD column. Successive observations are separated by the time it takes the star to cross from one fiducial line to the next (approx. 4.42 secs). We then adopt the first configuration, i.e. *tobs* of the NEP at the fiducial line of the first CCD column, on the first scan as the reference frame thereby obtaining the plate/CCD parameters that can 'transform' coordinates on any other frame onto this reference. In order to be consistent with observations of objects that fall on the 4th row of CCDs (where the last column CCD is replaced by a Wave Front Sensor), we use the first eight observing times obtained per AF transit due to the first 8 CCD columns (see Fig. 3).

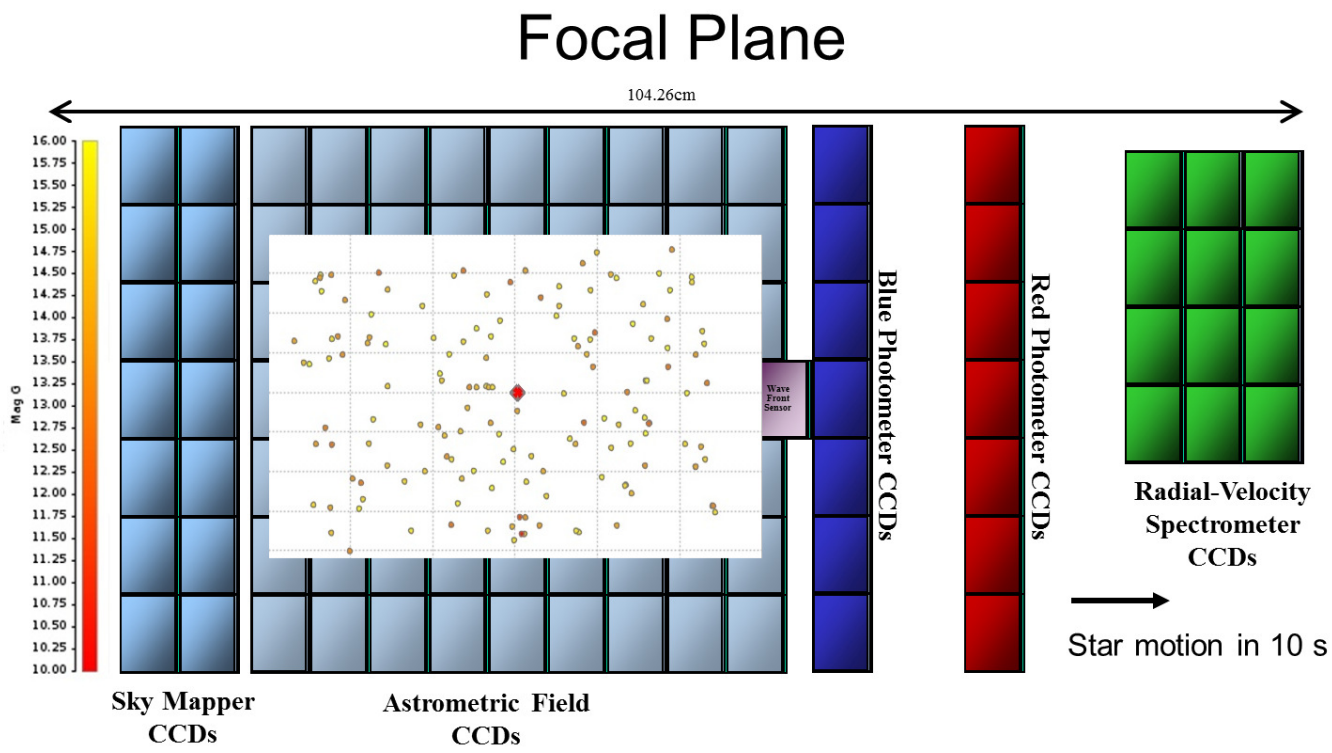

Figure 3. The Gaia focal plane showing the Astrometric, Red and Blue Photometers and RV Spectrometer alongwith the SkyMapper. The star field of interest is superposed on the focal plane and shows stars with G < 16 mag in a window of size 0.6X0.4 degrees around the north ecliptic pole shown in red and roughly in the middle of the Astrometric Field, i.e. the fifth CCD column, where each grid size is 0.1 degrees in the x-direction and 0.05 degrees in the y-direction. The stars are colour-coded according to their magnitudes given by the vertical colour bar shown on the left. Background image credit: ESA - A. Short.

Table 1. Standard uncertainties per CCD

Magnitude	σ per AL/AC observation
G = 10	71 μas/367 μas
G = 11	79 μas/411 μas
G = 12	60 μas/311 μas
G = 13	95 μas/493 μas
G = 14	151 μas/1603 μas
G = 15	240 μas/2642 μas
G = 16	383 μas/4950 μas

3. ACCURACY OF GAIA-LIKE SPACE-BASED ASTROMETRIC OBSERVATIONS

The measurements generally are affected by relativistic systematics such as velocity aberration and gravitational light deflection, and by the proper motions and parallaxes of the sources which can be classified as physical effects. They are also subject to instrumental errors that would require accurate modeling of the instrument and its calibrations and distortions.

3.1. *Physical Effects*

3.1.1. *Relativistic effects*

The aberration is by far the dominant effect and is caused by the motion of the observer with respect to the barycenter of the solar system (Klioner & Kopeikin

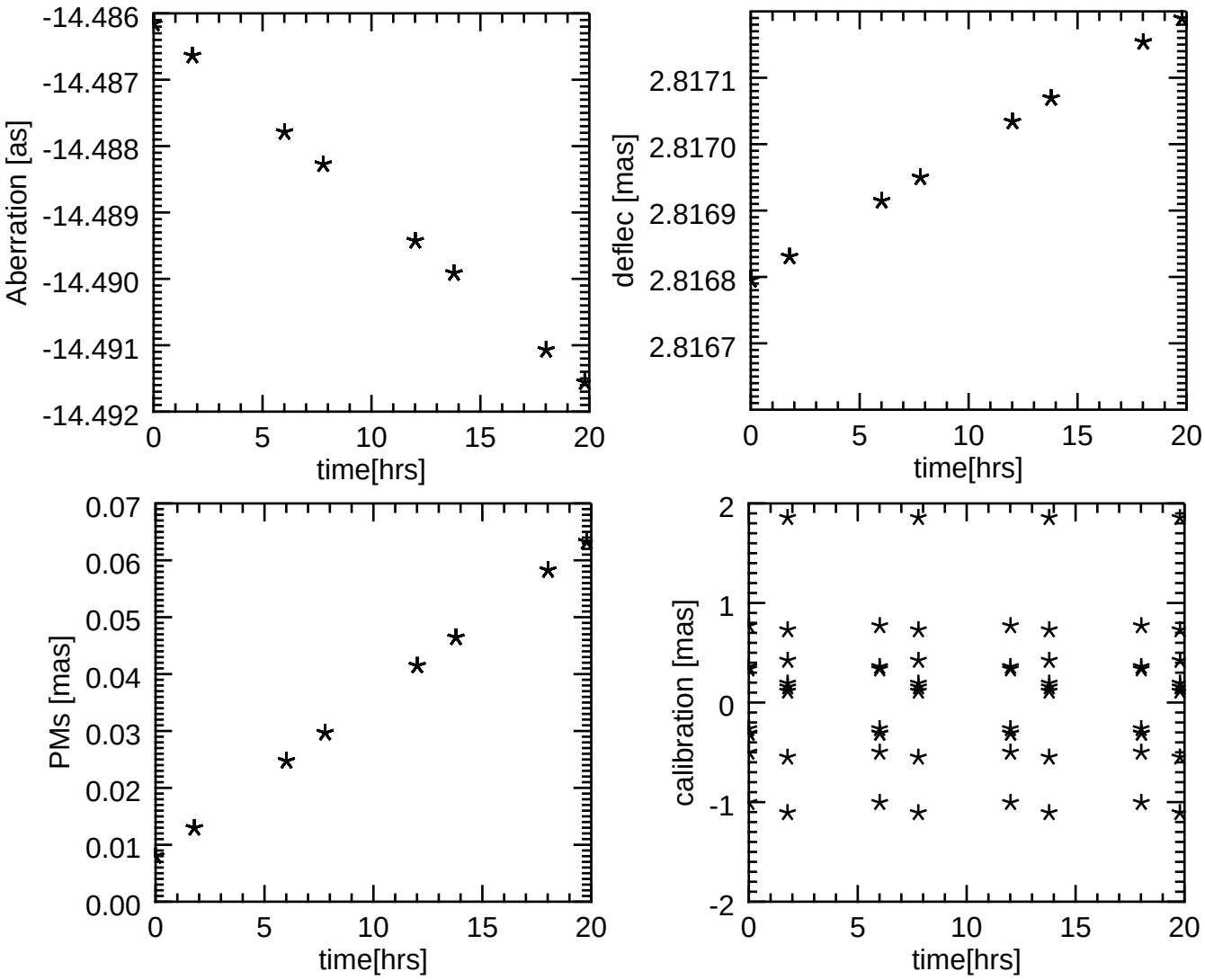

Figure 4. The time dependence of the Astrometric effects averaged over all stars in the sample. The top panels show the time dependence of the relativistic effects due to the aberration (left panel) and the gravitational deflection (right panel) whereas the lower panels show the equivalent effects due to the star's proper motion (left panel) and the geometric calibrations (right panel).

1992; Klioner 2003). This effect can be expressed as:

$$\delta\theta_{ab} = \frac{v}{c}\sin\theta\left[1+\frac{1}{c^2}(1+\gamma)w(x_0)+\frac{1}{4}\frac{v^2}{c^2}\right] - \frac{1}{4}\frac{v^2}{c^2}\sin 2\theta + \frac{1}{12}\frac{v^3}{c^3}\sin 3\theta + O(c^{-4}) \quad (1)$$

where θ is the angular distance between the direction to the target and the observers space velocity vector, v is the modulus of the BCRS space coordinate velocity of the observer, in this case Gaia, c is the speed of light, $w(x_0)$ is the gravitational potential of the solar system that can be approximated by the potential of the spherically symmetric Sun, and γ is the parameterized post-Newtonian (PPN) parameter. This is roughly of the order of v/c to first order. For the speed of Gaia ($\simeq$ 29.6 km/s) the maximum values (projected values along the AL direction) are roughly 20.3" to first order, $\sim$2.7 mas to second order, and 3rd order terms are $\sim 1\mu$as.

The gravitational deflection of light due to Solar System objects is another major effect that needs to be taken into account and depends on the angular separation between the Solar system body and the given source. This deflection due to the Sun is given by (Mis-

ner et al. 1973):

$$\delta\theta_{def} = (1+\gamma)\frac{GM}{c^2 R_0}\cot\frac{\phi}{2} \quad (2)$$

where ϕ is the Sun-source separation angle, G is the gravitational constant, R_0 is the distance between the observer and the Sun, M is the mass of the perturbing body. This amounts to $\sim$ 4 mas at the NEP as seen by an earth-based observer (Turyshev 2002), and $\sim$ 2.5 mas as seen by Gaia.

Over time scales of 24 hours the *differential* aberration amounts to several mas whereas the *differential* gravitational deflection (mainly due to the Sun's monopole) is sub-μas. This is shown in the top panels of Fig. 4 where we can see the strong linear dependence with time of the relativistic effects.

3.1.2. *Astrometric effects due to the star's proper motion*

The stars' proper motions for this particular selection can vary up to several hundreds of mas/yr and the differential effect due to them is of the order of tens of μas over 24 hours as can be seen in the lower left hand panel of Fig. 4. The IGSL input star catalog does not provide parallaxes and in this study they are not included in the modeling.

3.2. *Instrumental effects*

The observation lines, given by the fiducial lines mapped onto the tangent plane, are affected by the geometric instrument model describing the layout of the CCDs. This includes the physical geometry of each individual CCD and its configuration in the Focal plane assembly; the distortions and aberrations in the optical system; nominal values of the focal length and basic angle, Γ (see Lindegren et al. 2012, 2016 for extensive details). As the instrument can undergo changes during the mission, these effects are time dependent and can be classified into three broad categories:

1. Large-scale AL calibrations: thermal variations in the optics, detectors and supporting structures occuring on short time-scales and different for each FOV.

2. Small-scale AL calibrations: physical defects or imperfections in the individual CCDs that are expected to be stable over very long time scales, possibly over the whole mission duration.

3. Large-scale AC calibrations: same physical origin as for 1) above, but assumed to be constant on long time scales due to the more relaxed calibration requirement in the AC direction.

In the differential scenario and for this paper, we will only be concerned with the Large-scale AL and AC calibrations where the former could potentially vary over time scales of a day. For purposes of this paper, where we use high-cadence observations over a day, we can safely assume these large scale calibrations to be constant. The AL large-scale calibration is modeled as a low order polynomial in the across-scan pixel coordinate μ (that varies from 13.5 to 1979.5 across the CCD columns, Lindegren et al. 2012) and can be written as:

$$\eta_{fn}(\mu,t) = \eta_n^0 + \sum_{r=0}^{2}\Delta\eta_{rfn}L_r^*\left(\frac{\mu-13.5}{1966}\right) \quad (3)$$

where f is the field of view index, n is the CCD index and r is the degree of the shifted Legendre polynomial $L_r^*(\tilde{\mu})$ as a function of the normalized AC pixel coordinate ($\tilde{\mu}$). A similar equation holds for the AC large-scale calibrations. We will assume non-gated observations which is technically only valid for faint sources; brighter star observations involve as many as a dozen gates that would need to be calibrated. The time-dependence of the differential calibration can be seen in Fig. 4 with a $\sim$2 mas standard deviation due to the simulated calibrations per CCD (Lindegren et al. 2016).

Furthermore, sources brighter than G $\sim$ 13 magnitude will always be observed as two-dimensional images, and fainter stars are observed as purely 1-dimensional images in the AF as discussed in Sec. 2 where we will exclusively use the SM AC positional information.

4. APPLYING THE PRINCIPLES OF DIFFERENTIAL ASTROMETRY

We adopt a differential procedure that is based on the standard one for obtaining the astrometric positions of the measured coordinates of an image on a plate/frame through the so-called plate solution. That usually involves using the 'known positions' of the reference stars to determine the plate solution coefficients through a least squares adjustment and then applying the plate solution to obtain the corresponding coordinates of the target star on the frame (Kovalevsky & Seidelmann 2004). The inverse gnomonic projection then gives the desired astrometric coordinates of the star. Here we still use the basic principle of obtaining the plate, or, for the case of Gaia, a frame solution, that is then used to 'transform' the field angles on various FOVs to the reference FOV, akin to 'stacking' the various FOVs onto a common one.

We will use the field angles over several successive transits, for a maximum of 8 transits which translates into 24 hours (the crossing of a FOV represents one transit), and study the model as:

$$x_i' = F(\text{frame, source, instrument parameters}, x_i) + \textit{offset} \quad (4)$$

where x_i' is the reference frame coordinate in arcseconds, which can be taken as the first frame field angle and x_i is the 'measured' field angle on the other frames.

The overlapping frames are solved using the Gaussfit software (Jefferys et al. 1988) that is a computer program in its own computer language (similar to C) and that is especially designed for solving least squares and robust estimation problems. It provides a straightforward way to formulate different types of complex problems, for e.g. problems in nonlinear estimation, problems with multiple observations per equation of condition, problems with correlated observations etc. It also allows the user to specify a robust estimation method that is resistant to outliers in the data.

The standard reduction method is the generalized least squares algorithm of (Jefferys 1980) which allows for the types of problems mentioned above alongwith their proper constraints. For numerical stability the solution is obtained by Householder transformation designed to deal efficiently with overlapping-plate conditions.

5. THE ASTROMETRIC MODEL

We adopt polynomial equations for the frame model parameters to study the different effects outlined in Sec. 3. Following Eq. 4 from the previous section these are written as:

$$\begin{aligned} x' &= a + bx + cy + dxy + ex^2 + fy^2 \\ &\quad + F(\pi, \mu, CCD) \\ y' &= g + hx + iy + jxy + kx^2 + ly^2 \\ &\quad + F(\pi, \mu, CCD) \end{aligned} \tag{5}$$

where x and y are the measured positions of the star on **any** frame, and x', y' are the positions of the stars on the **reference** frame, and π, μ are respectively the source parallax and proper motion. All the measured quantities have their associated errors. As we are looking to solve the problem in a differential manner, we take one of the frames as the reference one, and the stars on the other frames are 'adjusted' to the reference one. The frame model equation then gives the fitted x', y' and consequently how well it describes the positions of the stars. Any significant deviation is an indication that the model needs to be changed and adapted to the science case at hand. With Gaussfit we can estimate the x & y variables alongwith all the plate constants simultaneously.

5.1. *Linear model*

As mentioned in Sec. 2 the observation time ranges around the NEP in each field of view of Gaia which then fixes the nearby distribution of stars subsequently simulating the field angles (η, ζ) for these stars. The linear 'plate model' is given by:

$$\begin{aligned} \eta_{ij}^{'} &= \eta_{ij} + \sum_{r=0}^{2} \Delta\eta_{rfnk} L_r^* (\frac{\mu - 13.5}{1966}) \\ \zeta_{ij}^{'} &= \zeta_{ij} + \sum_{r=0}^{2} \Delta\zeta_{rfnk} L_r^* (\frac{\mu - 13.5}{1966}) \\ \eta_{0j}^{'} &= a_i \eta_{ij}^{'} + b_i \zeta_{ij}^{'} + c_i - \mu_{\eta j} \Delta t_{ij} - P_\eta \pi \\ \zeta_{0j}^{'} &= d_i \eta_{ij}^{'} + e_i \zeta_{ij}^{'} + f_i - \mu_{\zeta j} \Delta t_{ij} - P_\zeta \pi \end{aligned} \tag{6}$$

where i is the frame number, and j is the star number. η_{0j} and ζ_{0j} are the reference field angles of the jth star measured in the reference field of view, whereas η_{ij} and ζ_{ij} are the measured nominal field angles of the jth star in the ith frame and their primed counterparts are the calibrated field angles. The constants a_i, b_i, d_i and e_i are scale and rotation plate constants, whereas c_i and f_i are offsets; $\mu_{\eta j}$, $\mu_{\zeta j}$ are the proper motions, π is the parallax, and P_η, P_ζ are the computed parallax factors and Δt_{ij} is the epoch difference between the ith frame star observation and the reference frame.

For now we will also assume that the stars have zero parallaxes mainly due to the zero input values from the IGSL catalog.

Gaussfit solves this set of equations through a least squares procedure that minimizes the sum of squares of the residuals constrained by the input errors alongwith appropriate constraints on the proper motions (Eichhorn 1988) and calibration parameters (Lindegren et al. 2012). The fitted plate/frame parameters (a through f) then gives the model whereby the observations (η_{ij}, ζ_{ij}) in any given frame can be 'transported' to a common reference frame. The distribution of residuals then informs us as to how well the model accounts for various physical or instrumental effects. It is found that a_i and e_i are almost unity, whereas $b_i = -d_i$ and together they give the rotation and orientation. The offsets c_i and f_i give the zero point of the common system.

5.1.1. *Astrometric Reference frame residuals*

The standard deviation of the residuals binned as a function of the star's G-magnitude is shown in Fig. 5 for simulations with the Gaia Relativistic Model (GREM, Klioner 2003) implementation and for a perfect instrument and zero proper motions superposed on the full model with all effects included as written in Eq. 6. The number of reference stars is intrinsically determined by the magnitude cut of the sample and gives us a rough lower limit that is already according to the useful rule of thumb where at least 3 times the number of observations is needed as coefficients to be determined.

With the addition of the geometric instrument model the number of parameters increases by a factor of 6x48x2 ([# of calibration parameters per CCD]×[# of CCDs per

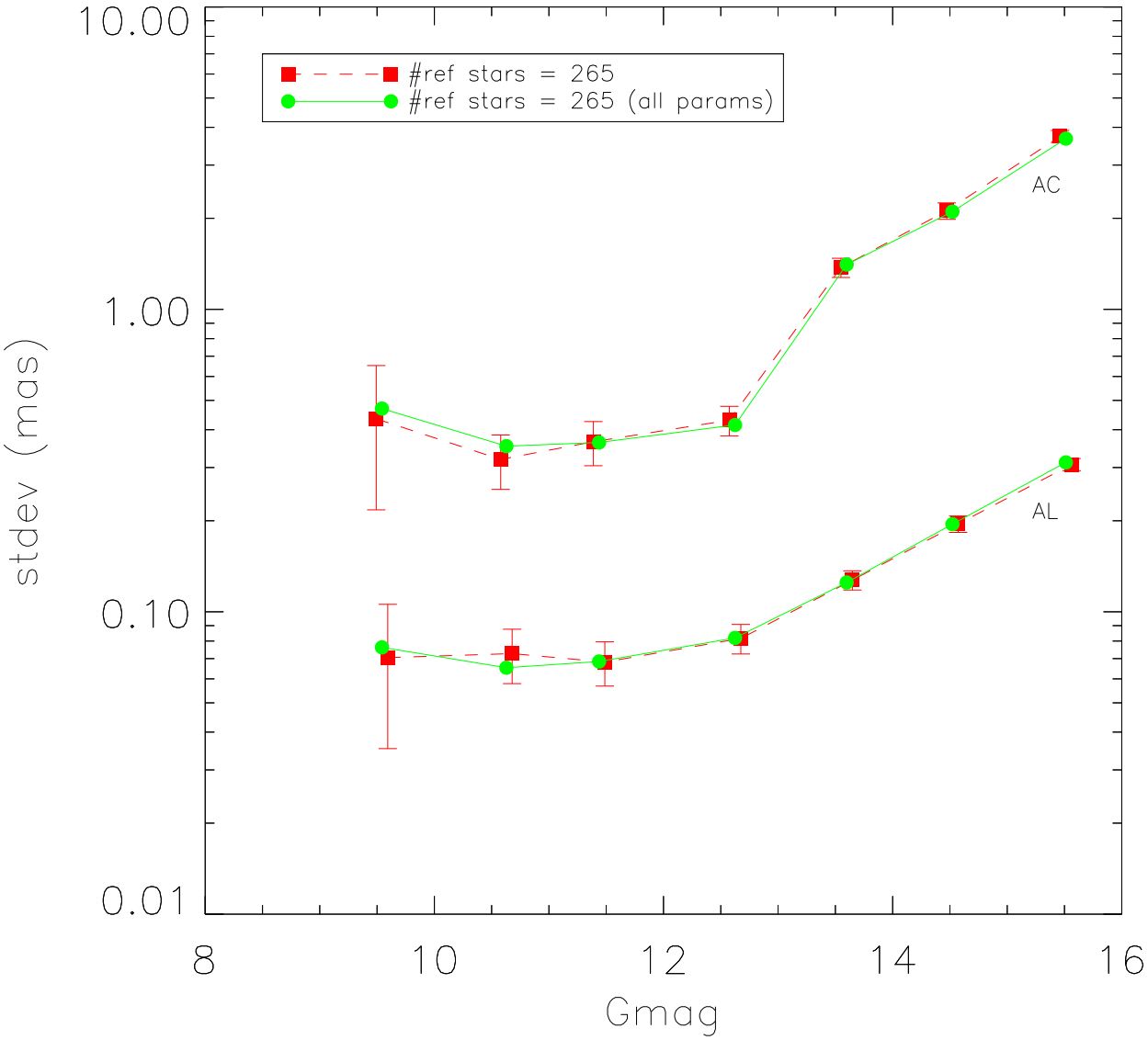

Figure 5. The standard deviations (in mas) from using a linear model to fit the overlapping frames of observations around the NEP in bins of the star's G-magnitude simulated with a perfect instrument and no proper motions (red dashed lines) superposed to the full linear model with all physical and instrumental effects included (green solid line). The lower and upper curves show the standard deviations in AL and AC respectively with input errors that follow the standard CCD-level location estimation errors. The error bars are poissonian (inversely proportional to the square root of the number of stars for that magnitude bin).

FOV]×[# of FOVs]) = 576 (see Eq. 3 and using 8 CCD columns as described in Sec. 2 with the added constraint of the offset between the two FOVs). For this particular simulation we have 8 frames per transit for a total of 8 transits over 24 hours providing us with 64 observations per star. The requirement would then be for at least 50 reference stars in order to reliably estimate the residuals and have a good coverage over the different CCDs.

We find a very good agreement as can be seen in Fig. 5 which implies that a fully linear model is sufficient to describe the various physical and instrumental effects.

The goodness of fit can be seen in the left panels of Fig. 6 that shows the histogram of the ratio of the residuals to the input standard uncertainties per AL/AC observation (Table 1) for the full G < 16 mag sample. The right panels show that brighter stars have smaller astrometric residuals, as expected. We further tested the robustness of the astrometric solution by performing two additional tests (not shown here) that confirmed a direct linear dependence of the standard deviation of reconstructed test positions with increasing input standard uncertainties and increasing distances from the center of the reference star sample.

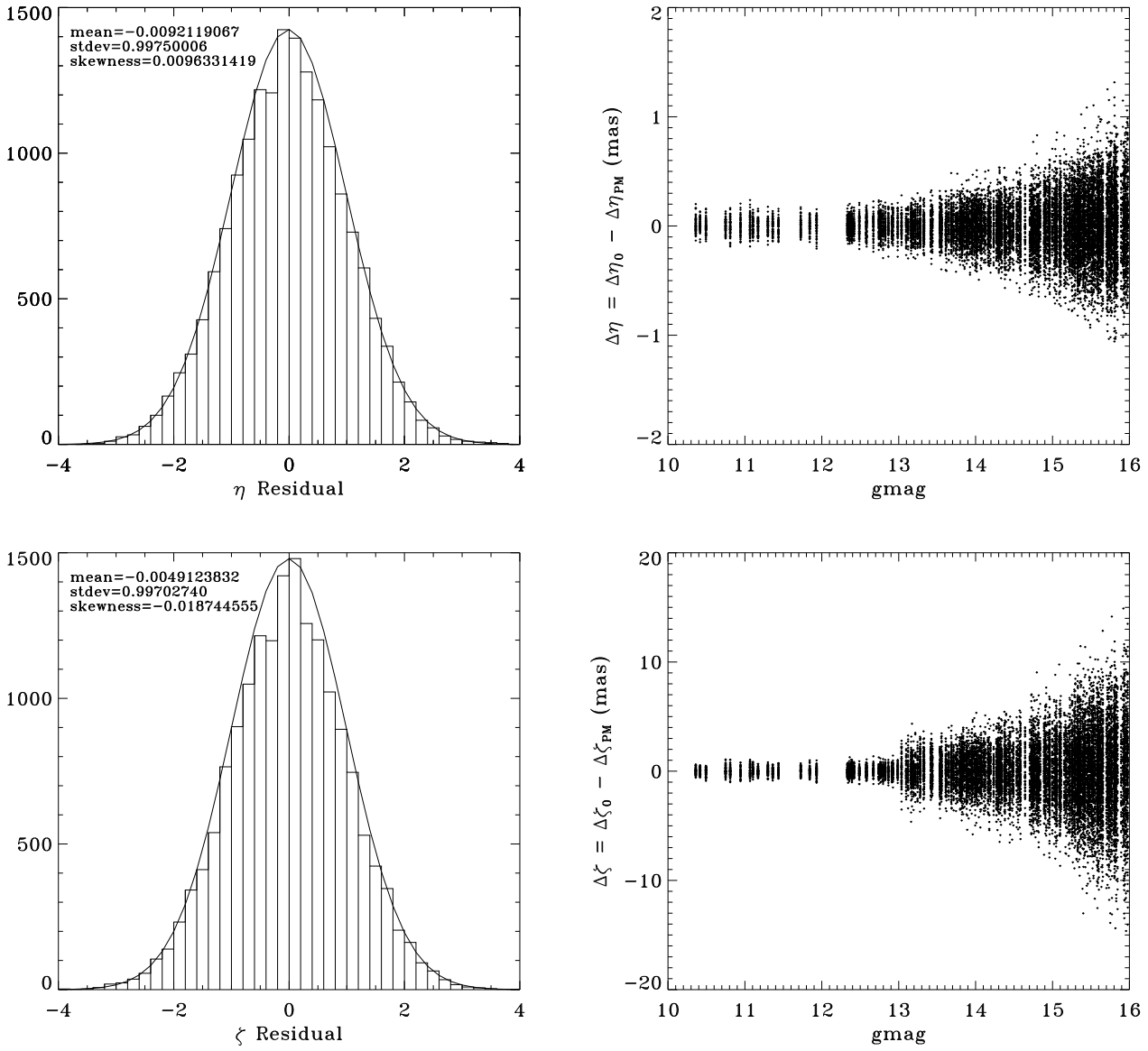

Figure 6. The histogram of the ratio of the estimated residuals and the input standard uncertainties (left panels) from using a linear model with proper motions and calibration parameters used to fit the overlapping frames of observations around the NEP for stars with G < 16 mag in the AL (top panel) and AC directions (bottom panel). The fitted gaussian distributions are shown as curves overlapping the histograms. The residuals follow a magnitude-dependent distribution (right panels) that is mainly driven by the input errors.

6. DISCUSSION

We have studied simulated observations of Gaia field angles (η and ζ) as measured in its FOV over short timescales of 24 hours within the framework of Differential Astrometry. In order to satisfy the requirement for a minimum number of reference stars needed to resolve the equations of condition we relied upon high-cadence simulated observations at the North Ecliptic Pole such as those obtained during the EPSL (described in Sec. 2). This allowed us to study the standard astrometric linear model with the inclusion of calibration parameters both in the AL and AC directions. The Gaia catalog essentially provides global astrometric products (celestial coordinates, proper motions and parallaxes) that are obtained with the AGIS (Astrometric Global Iterative Solution) process involving a highly time-consuming sphere solution. Instead, harnessing the power of differential astrometry we look at how the field angles can be used to construct a small field reference frame that can essentially be performed on any laptop without the need for supercomputers. This methodology would need to be applied to the observed field angles.

With a perfect instrument and no proper motions (only relativistic effects due to aberration and gravitational light deflection included) we can recover the μas stability of the reference frame with a modest number of stars ($\sim$ 37) down to the 13th G-magnitude for this particular field of interest. Including all astrometric effects due to physical and instrumental causes we require at least as many stars as the number of CCD's in the Gaia Focal Plane restricting us to samples with magnitude limits fainter than the 14th magnitude (i.e. <14, <15, <16). The stability is shown in Fig. 7 in the form of the differences between the standard deviations of the estimated residuals and the input standard uncertainties (Table 1) per magnitude bin. Moreover, the stability shows the capability of brighter stars in constraining better a target position due to their conventionally smaller standard uncertainties. It is remarkable that we are able to maintain the μas stability of the reference frame even with the inclusion of 576 more unknowns (see Sec. 5.1.1). As expected, the full linear model in AC is less stable due to the less precise positions in the AC direction as compared to the μas stability of the same model in AL.

Extra instrumental effects would have to be modeled as systematics and if left untouched would lead to a less stable small field reference frame. The present study represents a best case scenario to show that with a slightly more simplified geometric instrument model we are still able to recover a stable small field reference frame in the AL, less so in the AC direction. For real Gaia observations one needs to account for actual CCD gate and window effects and time dependencies (especially when looking at differential effects on time scales longer than just a day, see Lindegren et al. 2016 for more details). Other effects due to color, magnitude, and possibly, variations in the basic angle, would also need to be modeled and carefully accounted for in the final processing.

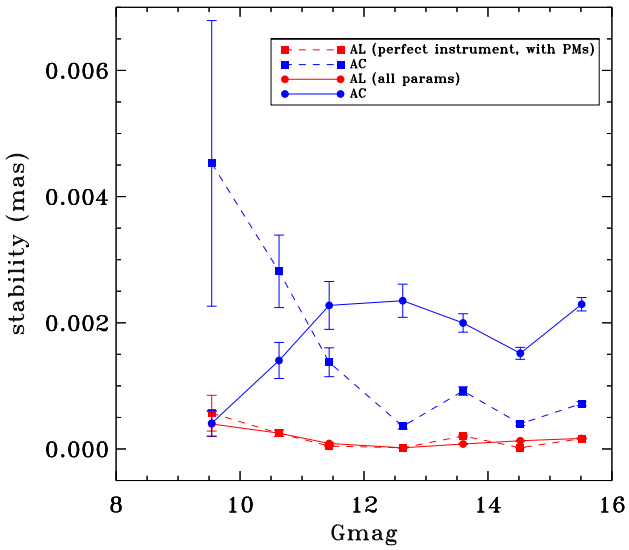

Figure 7. The stability (absolute differences between the standard deviations of the estimated residuals and the input standard uncertainties) of the Differential Astrometric Reference Frame in bins of the star's G-magnitude for different models in the AL and AC directions with poisson errors. The dashed lines are for a perfect instrument model (only physical effects included), whereas the solid lines are for the full linear model as given in Eq. 6. Red and blue lines are for the AL and AC scan directions respectively.

7. FUTURE PERSPECTIVES

Once all linear effects due to astrometric, i.e. physical and instrumental causes, are accounted for in the model and a stable reference frame has been established we can look at short and long-time effects that would need to be correctly modeled as a systematic effect in the differential scenario described. Possible experiments include:

7.1. *Relativistic Experiments*

7.1.1. *Gaia Relativistic Light Deflection Experiment on Jupiter's Quadrupole moment*

The nominal scanning law of Gaia after the EPSL was optimized in the initial parameters to favour events of bright stars close to the limb of Jupiter for the relativity light deflection experiment due to Jupiter's quadrupole moment (GAREQ - GAia Relativistic Experiment on Jupiter's Quadrupole moment, see Sec. 2).

Results based on simulated observations with a Galaxy model showed that Gaia can provide the

measurement of the light bending effect due to the quadrupole moment with a 3σ confidence level (Crosta & Mignard 2006). In that paper the quadrupole deflection has been parameterized by introducing a new parameter ϵ, equal to one if GR predictions are true. The total effect is formulated as a vectorial deflection angle, the sum of two contributions along the radial and orthoradial directions. This secondary deflection has a very specific pattern as a function of (i) the position of the star with respect to the oblate deflector and (ii) the orientation of its spin axis. A light ray grazing the limb of Jupiter would be subjected to a quadrupole induced deflection of $\sim$240μas superposed on a $\sim$16mas monopole term. The aim was to assess the detection of the light bending effect due to the quadrupole moment of Jupiter starting from the simplest case (no gravitodynamical effects, no instrument model), providing the groundwork for future developments. Due to the degradation of the astrometric accuracy, this first simulation showed that the inclusion of stars fainter than V = 16 does not improve the final precision on ϵ. Instead, by running the simulation on a selection of a few epochs that include the maximum number of bright stars, the results showed that a single experiment can do almost as well as the 5-year mission. This gave a vital sign that more detailed investigations on specific bright stars spots around Jupiter were in order. Subsequent simulations (Crosta et al. 2008a,b,c) with selected fields extracted from the GSCII data base, namely a real count of objects around Jupiter as observed by Gaia as a function of the star's magnitude and distance from Jupiter's edge, singled out how to further improve Gaia's ability to detect the quadrupole light deflection, that has been predicted yet never detected.

Due to the motion of Jupiter in its orbit such an event is short-lived and measurable above the μas level only for $\sim$20 hours for the most favourable events involving the same bright star (Gmag<12). The situation is further complicated by Gaia not necessarily 'seeing' the bright star on successive transits. Nonetheless, it will be interesting to see the confidence level of such effects on short time scales and will be the subject of future investigations.

7.1.2. *Astrometric Gravitation Probe project*

Techniques of differential astrometry like the one described in this work and developed for the GAREQ experiment can be conveniently applied in other astrometric experiments involving astrometric tests of gravity theories. One significant example in this sense is the Astrometric Gravitation Probe (AGP) project (Vecchiato et al. 2015; Gai & et al. 2015), a concept for a space mission whose main scientific goal is the determination of the γ and β parameters of the PPN framework at the $\sim 10^{-8}$ and $\sim 10^{-6}$ level respectively. In particular, the estimation of β would be obtained by an astrometric reconstruction of the orbit of Mercury, and possibily of some selected NEOs. Such reconstruction, requiring the determination of the ephemerides of the observed objects with respect to the background stars, is clearly based on techniques of differential astrometry. It is also expected that such objects will be observed repeatedly in partially overlapping small fields, thus repeating the kind of situation investigated in this work. Moreover, another possible application of AGP is precisely a GAREQ-like observing scenario, for which a satellite scanning a small sky region is better suited with respect to Gaia.

7.2. *Extrasolar planets*

The promise of Gaia global astrometry in the exoplanet arena has been the objective of several studies in the past 15 years (e.g. Lattanzi et al. 2000; Sozzetti et al. 2001, 2014, 2016; Casertano et al. 2008; Perryman et al. 2014; Sahlmann et al. 2015). The development of a technique to extract and model very high-accuracy two-dimensional local astrometric measurements from the original one-dimensional Gaia data will allow to verify the existence of orbital motion induced by planetary-mass companions based on a different approach to the modeling of calibration and instrument attitude effects (the latter not treated in this work but of importance when considering time series with years-long time baselines). For systems for which a robust set of references can be established, such methodology could be particularly effective for the confirmation of astrometric signals corresponding to peculiar cases, such as edge-on, face-on, and highly eccentric orbits, and it might also help in the interpretation of Gaia data for very bright stars. The establishment of a robust framework for the proper modeling of narrow-field astrometry at the μas level will also be valuable in the perspective of future efforts to exploit the technique for detection of orbital motion induced by terrestrial planets in the Habitable Zone of the nearest solar-type stars (Malbet et al. 2012).

7.3. *Brown dwarfs*

In Gaia DR1 over 300 known ultracool later than L0 dwarfs have been found and from this it is estimated the final tally of L/T dwarfs directly visible to Gaia will be around 1000 (Smart et al, submitted). The binary fraction of L/T dwarfs has many published values from 10-70% (see Marocco et al. 2015, and references therein) and the systems visible to Gaia are all close so will often be resolveable. Very prominent examples are the nearby Epsilon Indi B A T1V+T6V binary (McCaughrean et al. 2004) and Luhman 16 a L7.5+T0.5 binary (Luhman 2013), in both cases the individual ob-

jects will be resolved by, and visible to, Gaia. We can use the narrow field differential astrometry described here to determine the orbits of these systems and to search for possible other unresolved companions such as a planet that has been hypothesised in the Luhman 16 system (Boffin et al. 2014). The precise determination of the binary fraction remains one of the largest unknowns in the determination of the brown dwarf luminosity function that in turn would provide one of the best constraints we have on current formation theories.

7.4. *Satellite Tracking*

Another possible application is in the completely different observing scenario of the Satellite Tracking Astrometric Network (STAN). As explained in Vecchiato & Gai (2015), this project proposes the exploitation of a network of new or existing ground-based telescopes, which will be able to improve the orbit tracking of different types of satellites around the Earth. Their orbits will be determined by a continuous monitoring of their positions in sky with respect to background stars, whose positions are known with very high precision thanks to the forthcoming Gaia catalogue. Each satellite will be observed contemporarily from different positions from the ground, so, once again, on partially overlapping small astrometric fields.

We would like to thank the anonymous referee for several useful comments that helped to further improve the paper and tests that confirmed the robustness of the astrometric solution. This work was supported by the Italian Space Agency through Gaia mission contracts - The Italian participation to DPAC, ASI 2014-025-R.0 and 2014-025-R.1.2015 in collaboration with the Italian National Institute of Astrophysics.

REFERENCES

Benedict, G. F., McArthur, B. E., Fredrick, L. W., et al. 2002, AJ, 123, 473
Benedict, G. F., McArthur, B. E., Napiwotzki, R., et al. 2009, AJ, 138, 1969
Boffin, H. M. J., Pourbaix, D., Mužić, K., et al. 2014, A&A, 561, L4
Casertano, S., Lattanzi, M. G., Sozzetti, A., et al. 2008, A&A, 482, 699
Casertano, S., Riess, A. G., Anderson, J., et al. 2016, ApJ, 825, 11
Clementini, G., Ripepi, V., Leccia, S., et al. 2016, ArXiv e-prints, arXiv:1609.04269
Crosta, M., & Mignard, F. 2006, Classical and Quantum Gravity, 23, 4853
Crosta, M. T., Gardiol, D., Lattanzi, M. G., & Morbidelli, R. 2008a, in IAU Symposium, Vol. 248, A Giant Step: from Milli- to Micro-arcsecond Astrometry, ed. W. J. Jin, I. Platais, & M. A. C. Perryman, 395–396
Crosta, M. T., Gardiol, D., Lattanzi, M. G., & Morbidelli, R. 2008b, in EAS Publications Series, Vol. 30, EAS Publications Series, ed. A. Oscoz, E. Mediavilla, & M. Serra-Ricart, 387–387
Crosta, M. T., Gardiol, D., Lattanzi, M. G., & Morbidelli, R. 2008c, in The Eleventh Marcel Grossmann Meeting On Recent Developments in Theoretical and Experimental General Relativity, Gravitation and Relativistic Field Theories, ed. H. Kleinert, R. T. Jantzen, & R. Ruffini, 2597–2599
de Bruijne, J., Siddiqui, H., Lammers, U., et al. 2010, in IAU Symposium, Vol. 261, Relativity in Fundamental Astronomy: Dynamics, Reference Frames, and Data Analysis, ed. S. A. Klioner, P. K. Seidelmann, & M. H. Soffel, 331–333
Dinescu, D. I., Girard, T. M., van Altena, W. F., Mendez, R. A., & Lopez, C. E. 1997, AJ, 114, 1014
Eichhorn, H. 1988, ApJ, 334, 465
Gai, M., & et al. 2015, in Metrology for Aerospace (MetroAeroSpace), 2015 IEEE, pp. 329 - 334, 2015, 329–334
Gaia Collaboration, Prusti, T., de Bruijne, J., Brown, A., Vallenari, A., & co authors. 2016, A&A, 1609.04153v1
Holl, B., Lindegren, L., & Hobbs, D. 2012, A&A, 543, A15
Jefferys, W. H. 1980, AJ, 85, 177
Jefferys, W. H., Fitzpatrick, M. J., & McArthur, B. E. 1988, Celestial Mechanics, 41, 39
Johnston, K. J., & de Vegt, C. 1999, ARA&A, 37, 97
Klioner, S. A. 2003, AJ, 125, 1580
Klioner, S. A., & Kopeikin, S. M. 1992, AJ, 104, 897
Kovalevsky, J., & Seidelmann, P. K. 2004, Fundamentals of Astrometry, ed. C. U. Press (Cambridge University Press), 420
Lattanzi, M. G., Spagna, A., Sozzetti, A., & Casertano, S. 2000, MNRAS, 317, 211
Lindegren, L., & Bastian, U. 2011, in EAS Publications Series, Vol. 45, EAS Publications Series, 109–114
Lindegren, L., Lammers, U., Hobbs, D., et al. 2012, A&A, 538, A78
Lindegren, L., Lammers, U., Bastian, U., et al. 2016, ArXiv e-prints, arXiv:1609.04303
Luhman, K. L. 2013, ApJL, 767, L1
Malbet, F., Léger, A., Shao, M., et al. 2012, Experimental Astronomy, 34, 385
Marocco, F., Jones, H. R. A., Day-Jones, A. C., et al. 2015, MNRAS, 449, 3651
McArthur, B. E., Benedict, G. F., Harrison, T. E., & van Altena, W. 2011, AJ, 141, 172
McArthur, B. E., Benedict, G. F., Lee, J., et al. 1999, ApJL, 520, L59
McCaughrean, M. J., Close, L. M., Scholz, R.-D., et al. 2004, A&A, 413, 1029
Misner, C. W., Thorne, K. S., & Wheeler, J. A. 1973, Gravitation, ed. W. Freeman & Co. (W.H. Freeman and Co.)
Perryman, M., Hartman, J., Bakos, G. Á., & Lindegren, L. 2014, ApJ, 797, 14
Riess, A. G., Casertano, S., Anderson, J., MacKenty, J., & Filippenko, A. V. 2014, ApJ, 785, 161
Sahlmann, J., Triaud, A. H. M. J., & Martin, D. V. 2015, MNRAS, 447, 287
Smart, R. L., & Nicastro, L. 2014, A&A, 570, A87
Sozzetti, A. 2005, PASP, 117, 1021
Sozzetti, A., Bonavita, M., Desidera, S., Gratton, R., & Lattanzi, M. G. 2016, in IAU Symposium, Vol. 314, Young Stars & Planets Near the Sun, ed. J. H. Kastner, B. Stelzer, & S. A. Metchev, 264–269

Sozzetti, A., Casertano, S., Lattanzi, M. G., & Spagna, A. 2001, A&A, 373, L21
Sozzetti, A., Giacobbe, P., Lattanzi, M. G., et al. 2014, MNRAS, 437, 497
Treuhaft, R. N., & Lowe, S. T. 1990, in IAU Symposium, Vol. 141, Inertial Coordinate System on the Sky, ed. J. H. Lieske & V. K. Abalakin, 253–259
Turyshev, S. G. 2002, ArXiv General Relativity and Quantum Cosmology e-prints, gr-qc/0205061
van Altena, W., Anderson, J., Benedict, G. F., et al. 2013, Astrometry for Astrophysics, ed. C. U. Press (Cambridge University Press)
Vecchiato, A., Fienga, A., Gai, M., et al. 2015, IAU General Assembly, 22, 2247746
Vecchiato, A., & Gai, M. 2015, IAU General Assembly, 22, 2236451
Zverev, M. S. 1976, Soviet Astronomy Letters, 2, 83